MODELLING PRODUCTION FROM SUPERCRITICAL GEOTHERMAL RESERVOIRS

Edy Sudarmadi[1], Sadiq J. Zarrouk[2*], Adrian Croucher[2] and Eko Agung Bramantyo[1]

[1]Pertamina Geothermal Energy, Indonesia

[2] Department of Engineering Science, The University of Auckland, New Zealand

[*]s.zarrouk@auckland.ac.nz

Keywords: Supercritical, geothermal, numerical model, production.

ABSTRACT

As the opportunities for developing further conventional geothermal resources become increasingly limited, the development of deep supercritical reservoirs is attracting more interest. If the associated exploration, modelling and engineering challenges can be addressed, supercritical reservoirs represent a potentially large and untapped source of high-enthalpy fluid for power generation.

To investigate production from supercritical reservoirs, a simple idealized two-dimensional numerical model has been developed, using a supercritical version of TOUGH2 simulator. The model is 7 km deep and produces fluid from 4 – 5 km, a reasonable drillable depth. Numerical experiments indicated that steady-state supercritical conditions at this depth will be found only when permeability below it is low, of the order of 0.1 mD.

Simulations of production showed that reservoirs with higher porosity will give higher mass flows but lower flowing enthalpy, as expected. They also showed that, as in conventional reservoirs, mass flows in the well decline over the production period. However, unlike conventional liquid dominated reservoirs, the enthalpy of fluid produced from the supercritical reservoir also declines over time, from around 3100 kJ/kg to 2500 kJ/kg over 30 years. This is a result of the low permeability, which means the upflow zone is relatively narrow. As a result, cold fluid is drawn in more quickly over the production period. This also suggests that drilling for supercritical resources will need to target the upflow zone very accurately and that only high enthalpy (low permeability) geothermal systems should be considered.

1. INTRODUCTION

1.1 Background

A fluid is called 'supercritical' when temperatures and pressures are high enough that there is no longer any distinction between its liquid and vapour phases. Supercritical fluids are receiving increased attention generally due to their special properties and many possible industrial applications, ranging from extraction, particle formation, reactions and cleaning, in fields as diverse as food products, special lubricants, pharmaceuticals, paints and coatings, foams and aerogels (Fukushima, 1999). Water is the most widely used supercritical fluid, followed by carbon dioxide, helium and refrigerant (Pioro and Duffey, 2007).

Supercritical water occurs naturally in deep underground reservoirs, where minerals in aqueous solutions near or above the critical point have existed for billions of years. The process that forms these minerals is known as the hydrothermal process, and it has been widely used in the industrial production of high-quality single crystals (mainly gem stones) such as sapphire, tourmaline, quartz, titanium oxide, zircon and others (Levelt Sengers, 2000).

Apart from the applications mentioned above, supercritical water in geothermal reservoirs is of great interest, as it has the potential to reduce the cost of electricity generation through major improvements in the power output of geothermal wells (Fridleifsson et al, 2003). Development of supercritical geothermal reservoirs has been carried out by a consortium of companies in Iceland for the last decade. This program is called the Iceland Deep Drilling Program (IDDP). The main objective of this program is to produce supercritical fluids for electric power generation, with significantly higher enthalpies and flow rates than are currently found in conventional geothermal fields (Fridleifsson et al, 2003).

Supercritical conditions in pure water are reached when temperatures and pressures are higher than 373.95 ^{o}C and 220.64 bar respectively (referred to as the 'critical point').

	Conventional Dry steam well	**IDDP well**
Downhole temperature (^{o}C)	235	430 - 550
Downhole pressure (bar)	30	230 - 260
Volumetric rate of inflow (m^3/s)	0.67	0.67
Electric power output (MW_e)	~ 5	~ 50

Table 1: Comparison of conventional and unconventional geothermal systems (Fridleifsson, 2011).

The power output estimate in Table 1 is close to that expected from the enthalpy of supercritical water. The pressure and enthalpy diagram in Figure 1 shows the difference between conventional and deep wells in term of power produced.

Figure 1 also shows the process of decompression from a supercritical reservoir in a geothermal system into hot water with or without boiling (A-E and A-L). This situation represents high-temperature water-dominated geothermal reservoirs where boiling (typically induced by decompression) drives a thermo-artesian flow in a wellbore. The process from H-D is adiabatic decompression and it is a representation of a vapour-dominated geothermal reservoir. The basic idea of deep well development is to

bring supercritical fluid to the surface in such a way that it is transformed directly to superheated steam along a path like F-G. This process will result in power output much greater than that of conventional geothermal wells (A-E, A-L), possibly by an order of magnitude.

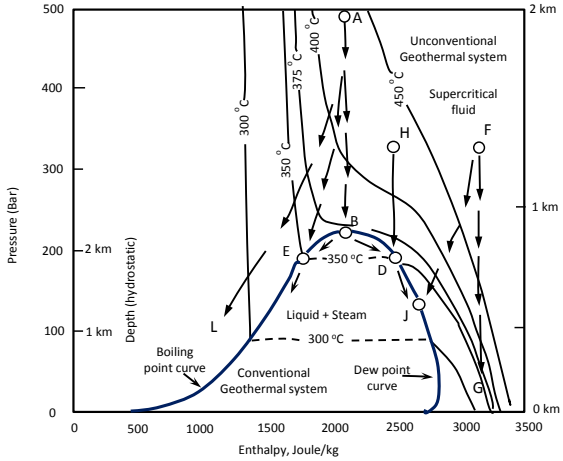

Figure 1: Pressure-Enthalpy diagram of water (Fournier, 1999).

1.2 Silica solubility in supercritical water

Geothermal fluids mostly come from recycled rain water, although a small amount of geothermal water may be derived from gases that were originally dissolved in magma (molten rock that is the source of volcanic eruptions and intrusive rocks). Water descends through faults to considerable depths, and water is stored in suitably porous and permeable rocks called aquifers. At a certain depth, water-rock interaction occurs because of high pressures and temperatures.

Rocks generally dissolve only slowly in water, but like most reactions this dissolution occurs more readily at higher temperatures. The equation below describes the reaction between water and rocks which produces clay and silica.

$$2H^+(aq) + 2KAlSi_3O_8(Feldspar) + 9H_2O \rightarrow 2K^+(aq) + Al_2Si_2O_5(OH)_4(kaolinite) + 5H_4SiO_4(dissolved\ silica)$$

A knowledge of the solution of SiO_2-H_2O (H_4SiO_4) in the hydrothermal process is necessary to overcome problems encountered when a supercritical well is put into production. Brunner (2009), Anderson & Burnham (1965) and Wood (1958) investigated the solubility of silica in water under supercritical conditions. Anderson & Burnham (1965) described the reaction of silicic acid:

$$SiO_2\ (Quartz) + 2H_2O \Leftrightarrow H_4SiO_4\ (Silicic\ Acid)$$

The solubility behaviour of silica in water can be seen in Figure 2. It changes significantly near the critical temperature. At relatively low pressure, the solubility drops nearly to zero as temperature increases. At higher pressure, however, the solubility climbs significantly as temperature increases.

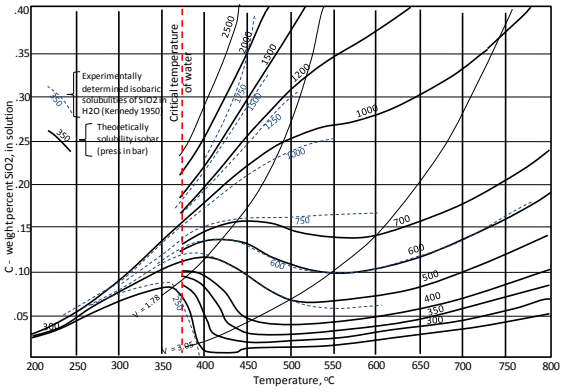

Figure 2: Experimental and theoretical solubility of silica in water (Wood, 1958).

2. OBJECTIVE

In this work, numerical modelling is carried out of production from an idealised geothermal reservoir under supercritical conditions. The reservoir simulator used is a modified version of AUTOUGH2 with supercritical capability (Croucher and O'Sullivan, 2008). The main objective is to estimate the production enthalpy and mass flow, together with their sensitivities to model parameters. This enables better estimates to be made of potential power output from production wells in supercritical reservoirs.

3. MODEL SETUP

A simple idealised reservoir is considered for this study, consisting of formations of homogeneous porous media. The model extends to a depth of 7 km, deep enough to enclose the convection plume. The zone at 4 – 5 km depth is targeted for production, as this is considered a feasibly drillable depth at which supercritical conditions may be encountered.

A simple two-dimensional rectangular 'vertical slice' model configuration was used (Figure 3). The main parameter values are listed in Table 2.

Length of model	9.9 km
Depth of model	7 km
Number of layers	70
Horizontal thickness	1 km
Block size	100 x 1000 x 100 m
Number of blocks	6930
Heat input	1.5 W/m^2

Table 2: Numerical model parameters.

Ambient atmospheric pressure and temperature boundary conditions are applied at the top surface. At the base of the model, heat sources are applied uniformly over the central 30 blocks. At the sides of the model, no boundary conditions are applied, which in TOUGH2 corresponds to no-flow boundaries. This is appropriate provided the model is large enough to enclose the convection plume with sufficient margin that flows near the lateral boundaries are small.

The model was used to carry out simulations of both natural state and a production scenario, as described below.

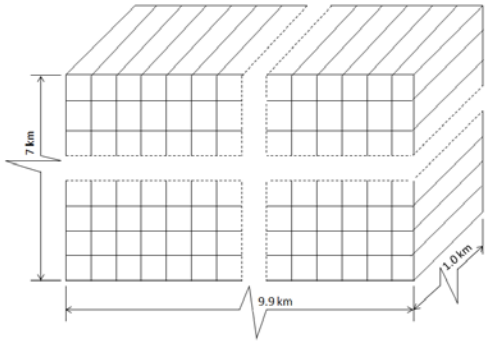

Figure 3: Numerical model geometry.

4. RESERVOIR SIMULATION

4.1 Natural state model

The natural state model was used to investigate reservoir properties (porosity and permeability) that give rise to supercritical conditions, prior to production.

The model divided the 70 layers into four types of rocks: breccia, cap rock, ignimbrite and deep rock (two varieties). The initial rock properties and assignments are shown in Table 3. Production is targeted at 4 – 5 km which is within the 'deep rock 1' formation.

Rock type	Porosity (%)	Permeability x, z (mD)	Depth (km)
Breccia	15	6.5, 2	0 – 1.5
Cap rock	3	0.001, 0.1	1.5 – 2.4
Ignimbrite	10	6.5, 11	2.4 – 3.9
Deep rock 1	5	10, 10	3.9 – 6.9
Deep rock 2	5	0.1, 0.1	6.9 – 7.0

Table 3: Rock properties for initial model.

For these parameters, the resulting steady-state temperatures are shown in Figure 4. This shows that at depths of 4 – 5 km, modelled pressures do exceed the critical pressure (221 bar), but temperatures do not reach the critical temperature (374 ^{o}C).

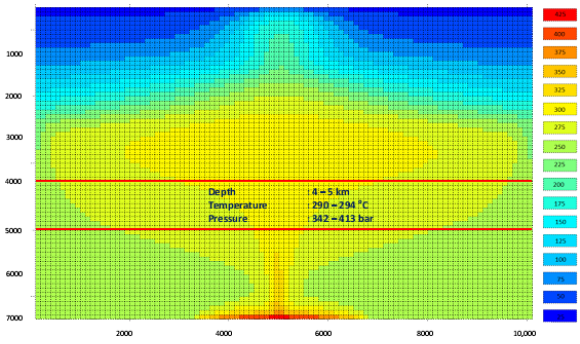

Figure 4: Modelled temperatures for 5% porosity and 10 mD permeability in the reservoir block (initial model).

Figure 5 shows the temperature and pressure profiles at the centre of the upflow zone. In this figure, the boiling point with depth (BPD) after the critical point (CP) is assumed to increase by 100 ^{o}C/km (Fridleifsson, 2011).

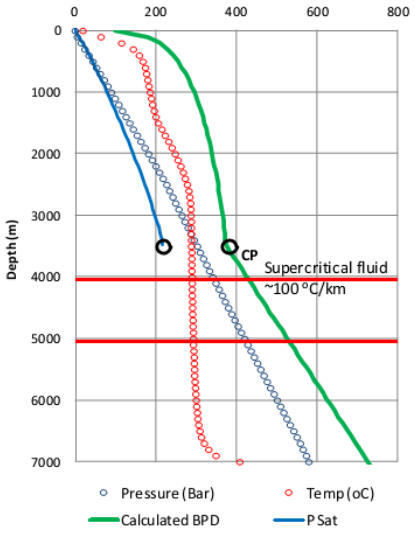

Figure 5: Pressure and temperature profiles in the upflow zone for 5% porosity and 10 mD permeability (initial model).

Again, it can be seen that supercritical conditions did not occur in the targeted production zone for these model parameters. Accordingly, the properties of the 'Deep rock 1' rock type were varied to investigate what values are needed for supercritical conditions to occur. Eight configurations of porosity and permeability were simulated. Table 4 summarises these configurations and the resulting modelled temperatures and pressures at depths of 4 - 5 km.

Model	Porosity (%)	Permeability (mD)	Temp. (^{o}C)	Pressure (bar)
initial	5	10	290 – 294	342 – 413
1	5	0.5	271 – 308	358 – 439
2	5	0.1	328 – 428	354 – 431
3	3	10	292 – 295	341 – 412
4	3	0.5	269 – 306	359 – 440
5	3	0.1	332 – 427	352 – 430
6	10	10	306 - 308	337 - 405
7	10	0.5	280 - 315	356 - 436
8	10	0.1	336 - 427	353 - 431

Table 4: Steady-state temperatures and pressures for all models.

From these results it can be seen that the only three models giving supercritical temperatures (T > 374 ^{o}C) in the production zone are models 2, 5 and 8, which are those with permeability 0.1 mD (regardless of porosity).

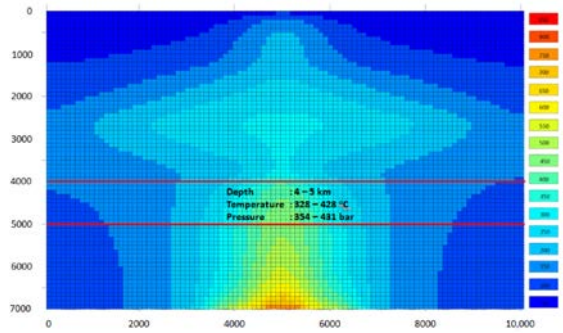

Figure 6: Modelled temperatures for 5% porosity and 0.1 mD permeability in the reservoir block (model 2).

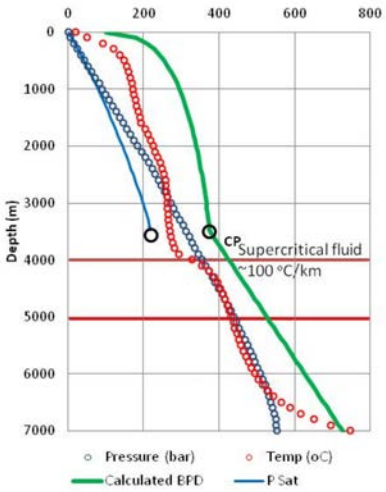

Figure 7: Pressure and temperature profiles in the upflow zone for 5% porosity and 0.1 mD permeability (model 2).

Figures 6 and 7 show the steady-state temperatures and temperature and pressure profiles in the upflow zone for model 2. Here it can clearly be seen that supercritical conditions have been reached in the production zone. Note also the shape of the temperature plume which is much narrower than that for the initial model.

4.2 Production scenario

The production scenario model is derived from steady state model 2 (see Table 4), which gave supercritical temperatures at a depth of 4 – 5 km. The production scenario was used to estimate the production mass flow and flowing enthalpy, together with their sensitivities to model parameters.

A single production well was introduced in the upflow zone at the centre of the model. Production was carried out for 30 years. The production well was simulated under deliverability, so that it produced against a prescribed flowing bottom-hole pressure P, with a productivity index PI (Pruess, et al, 1999). With this option, the mass flow rate of phase β from a grid block with phase pressure P_β > P_{wb} is :

$$q_\beta = \frac{k_{r\beta}}{\mu_\beta}\rho_\beta PI\left(P_\beta - P_{wb}\right)$$

For this model, the sensitivities of production mass flow and flowing enthalpy to three model parameters were investigated: porosity, bottom-hole pressure and productivity index.

4.2.1: Effect of porosity variation

Here, three values of reservoir porosity (3%, 5% and 10%) were used, while keeping the other parameters fixed (bottom-hole pressure P = 90 bar, productivity index PI = PI = 10^{-12} m^3).

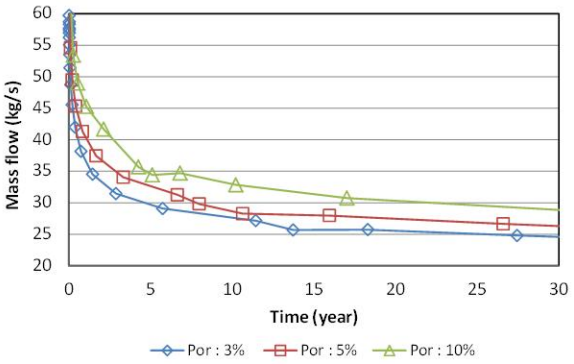

Figure 8: Production mass flow vs. time for three different porosity values.

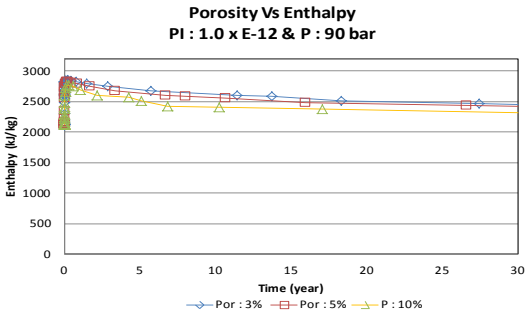

Figure 9: Flowing enthalpy (kJ/kg) vs. time for three different porosity values.

Figure 8 shows the production mass flow vs. time, for the three different porosity values. As expected, mass flows increase with increasing porosity.

Figure 9 shows the flowing enthalpy vs. time, again for the three porosity values. The enthalpy decreases with increasing porosity, again as expected, as there is more fluid to be heated in the porous medium.

4.2.2: Effect of bottom-hole pressure variation

Here, three values of bottom-hole pressure P (90, 100 and 110 bar) were used, while keeping the other parameters fixed (porosity = 3%, productivity index PI = PI = 10^{-12} m^3).

Figures 10 and 11 show the mass flow and flowing enthalpy over the production period for the three different

wellbore pressures. The effect of bottom-hole pressure is relatively small, but it can be seen that higher bottom-hole pressures slightly decrease both the mass flows and flowing enthalpies.

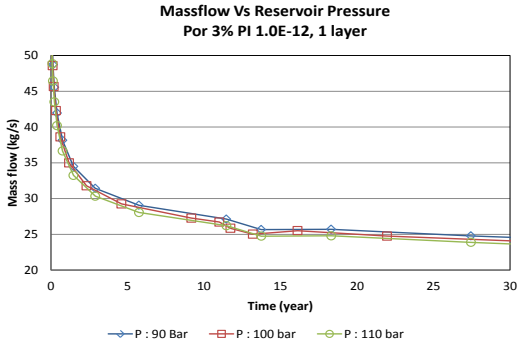

Figure 10: Production mass flow vs. time for three different bottom-hole pressure values.

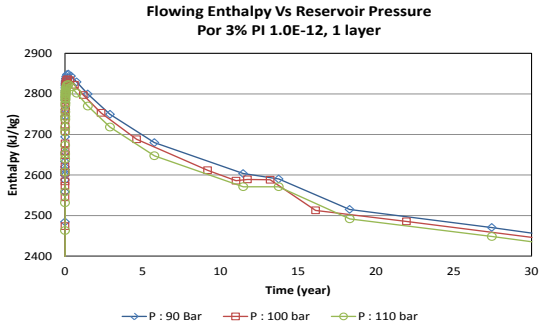

Figure 11: Flowing enthalpy (kJ/kg) vs. time for three different bottom-hole pressure values.

4.2.3: Effect of productivity index variation

Here, three values of productivity index PI (10^{-11}, 10^{-12}, and 10^{-13} m^3) were used, while keeping the other parameters fixed (bottom-hole pressure P = 90 bar, porosity = 3%).

Figures 12 and 13 show the mass flow and flowing enthalpy over the production period for the three different productivity indices. Clearly, higher productivity indices increase both the mass flow and flowing enthalpy.

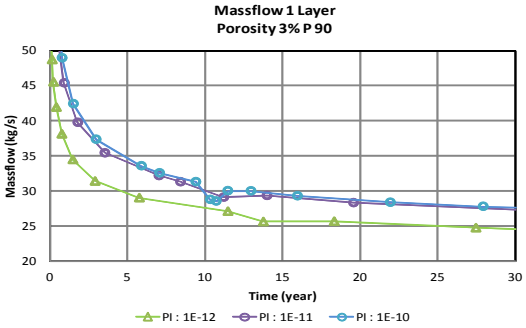

Figure 12: Production mass flow vs. time for three different productivity index values.

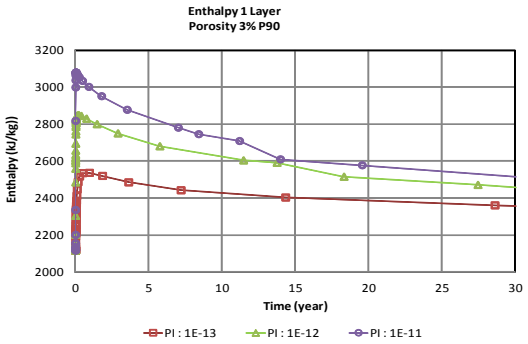

Figure 13: Flowing enthalpy (kJ/kg) vs. time for three different productivity index values.

5. DISCUSSION

The results of the natural state simulations indicate that low permeabilities (less than 0.1 mD) at depth are required before supercritical conditions will occur within the targeted production zone (4 – 5 km depth). As expected, porosity had little effect on the natural state results. At these low permeabilities, the temperature plume is narrow, only a few kilometres across, and areas of relatively cold water (less than 100 ^{o}C) can exist close to the plume even at depth. This has implications for exploration, as drilling for supercritical resources will have to target the upflow zone as accurately as possible (particularly given the added expense of drilling to greater depths). In addition, only high-enthalpy, low-permeability systems should be targeted.

The production simulations show that in many respects the behaviour of a well producing supercritical fluid is similar to that of a conventional well. At higher porosities, mass flows increase and flowing enthalpies decrease, as a result of the larger volumes of fluid contained within the pore space of the reservoir. Higher bottom-hole pressures result in slight increases in both mass flow and flowing enthalpy, while higher productivity indices give higher mass flows and flowing enthalpies.

Mass flows declined over the simulated supercritical production period, from around 50 kg/s to 25 kg/s over 30 years, which is again similar to the behaviour of conventional production wells. The flowing enthalpy, however, also declined over time, from around 3100 kJ/kg to 2500 kJ/kg. This is different from the typical behaviour of a conventional production well, in which enthalpy may increase over time as more steam is produced. In the supercritical case, the enthalpy decline is caused by the narrow temperature plume (which in turn is a result of the low permeability), which means that colder fluid is drawn in more quickly.

Taking these approximate figures for mass flow and flowing enthalpy, and applying an efficiency of conversion of 15%, we could expect the electric power output from a supercritical well to be of the order of 20 MW_e, declining to 10 MW_e after 30 years of production. This is not quite as high as the 50 MW_e suggested in Table 1, but the reservoir conditions in our model are not the same as those assumed in Table 1 (in particular, our modelled downhole temperatures are not as high). In addition, the model used

here is only two-dimensional, so the simulated mass flows cannot be taken as fully representative of an actual system.

REFERENCES

Anderson, G.M. and Burnham, C.W.: The solubility of quartz in supercritical water. *American Journal of Science*, 263, 494–511. (1965).

Brunner, G.: Near critical and supercritical water part I. Hydrolytic and hydrothermal process, Journal of Supercritical Fluid 47. pp. 373-381. (2009).

Croucher, A.E., and O'Sullivan, M.J.: Application of the computer code TOUGH2 to the simulation of supercritical conditions in geothermal systems. *Geothermics* 37. pp. 622-634. (2008).

Fournier, R.O.: Hydrothermal processes related to movement of fluid from plastic in brittle rock in the magmatic-epithermal environment, *Society of Economic Geologists*, California. (1999).

Fridleifsson, G.O., Ármannsson, H., Árnason, K., Bjarnason,I., Gíslason, G.: *Iceland Deep Drilling Project, Part I "Geosciences – site selection"*, IDDP Feasibility Report, Part I of III. (2003).

Fridleifsson, G.O.: *Iceland Deep Drilling Project: Drilling into Supercritical Geothermal Systems*, Overview 27-08-2011. IDDP. (2011).

Fukushima, Y.: *Application of Supercritical Fluid*. R & D review of Toyota CRDL, Vol.35 No.1. (1999).

Lovelt Sengers, J.M.H.L.: Supercritical fluids: their properties and applications. In *Supercritical Fluids*, E. Kiran et al. (Ed) NATO Advanced Study Institute on Supercritical Fluids – Fundamentals and Application, NATO Science Series E, applied Sciences, Kluwer Academic Publishers, Netherlands, Vol.366, pp. 1-29.

Pioro, I.L. and Duffey, R.B.: *Heat Transfer and Hydraulic Resistance at Supercritical Pressures in Power Engineering Applications*, ASME Press, New York, USA. (2007).

Pruess, K., Oldenburg, C. and Moridis, G.: *TOUGH2 User's Guide*, Version 2.0. Report LBNL-43134, Earth Sciences Division, Lawrence Berkeley National Laboratory, University of California, Berkeley, California. (1999).

Wood, J. A.: The solubility of quartz in water at high temperatures and pressure, *American Journal of Science*, vol. 256. (1958).